



ISARD (v1.0): A Reproducible Geostatistical Framework for Daily Precipitation Ensemble in Mountainous Terrain

Valentin Dura^{1,2}, Guillaume Evin², Anne-Catherine Favre², and David Penot¹

Correspondence: Valentin Dura (valentin.dura@edf.fr)

Abstract.

Gridded precipitation datasets are essential for hydrological and climate applications. However, commonly used products suffer from systematic biases such as seasonal total underestimations in mountainous regions and excessive smoothing of the spatial variability of extremes. Here, we present a reproducible workflow for generating a daily precipitation ensemble, conditioned on rain gauges, at 1 km resolution for mountainous regions. The approach leverages climatological information and spatial variability from Convection-Permitting Regional Climate Model (CP-RCM) simulations. The workflow corrects raingauge undercatch, incorporates CP-RCM-based climatology to improve seasonal totals, and estimates anisotropic variograms from CP-RCM daily fields to capture directional precipitation structures. Finally, Sequential Trans-Gaussian Simulations generate the daily ensemble of 100 members. We evaluate commonly used gridded precipitation products and the proposed approach using independent evaluation data, including in-situ measurements in mountainous areas (snow water equivalent, glacier mass balances, streamflow), regional catchment-scale water balance models, and hydrological models. Results demonstrate that our framework outperforms deterministic gridded products. First, it more accurately captures seasonal totals in highaltitude Snow Water Equivalent (SWE) and glacier observations, and reproduces both seasonal precipitation amounts and their interannual variability. Second, the daily ensemble captures fine-scale spatial variability and quantifies interpolation uncertainty, improving flood hydrological modelling. The workflow is fully reproducible via open-source code, transferable to regions with sparse rain-gauge networks or limited radar coverage. Beyond precipitation, it is adaptable to other climate variables simulated by weather models.

1 Introduction

Daily gridded precipitation datasets are essential for a wide range of applications, including snowpack modeling (Quéno et al., 2016), glacier mass balance assessments (Vionnet et al., 2019), hydrological modeling (Evin et al., 2024), or climate model evaluation (Fantini et al., 2018). While rain gauges primarily measure precipitation, their sparse and uneven distribution, especially in mountainous regions, limits their ability to capture spatial variability (Hofstra et al., 2010). Interpolating these point measurements onto regular grids is therefore necessary, but particularly challenging in complex terrain due to strong orographically induced gradients (Dura et al., 2024b) and localized extremes.

¹EDF-DTG, Grenoble, France

²Univ. Grenoble Alpes, CNRS, INRAE, IRD, Grenoble INP*, IGE, 38000 Grenoble, France

^{*}Institute of Engineering and Management Univ. Grenoble Alpes



40



Several categories of gridded precipitation datasets exist, each with its specific strengths and limitations, particularly when 25 applied to mountainous hydrology. Atmospheric reanalyses, including The Copernicus European Regional ReAnalysis Land (CERRA-Land, Le Moigne, 2021), the Système d'Analyse Fournissant des Renseignements Adaptés à la Nivologie (SAFRAN, Vidal et al., 2010), offer physically consistent long-term records but remain limited by their coarse resolution, smoothing of orographic effects (Dura et al., 2024b), and underestimation of extremes. Radar-based datasets such as COmbinaison en vue de la Meilleure Estimation de la Précipitation HOraiRE (COMEPHORE, Champeaux et al., 2009) or CombiPrecip (Sideris et al., 2014) capture the small-scale variability of extremes. However, ground echoes, beam blockage, and bright-band contamination (e.g. Berne and Krajewski, 2013) cause large seasonal total underestimations (Faure et al., 2019; Gugerli et al., 2020), limiting their application in mountain environments. Gauge-based interpolation products such as SPAZM (Gottardi, 2009), and SPARTACUS (Hiebl and Frei, 2018) offer an improved mountain climatology representation using climatological background fields (Masson and Frei, 2014; Jiang et al., 2023), but remain affected by sparse gauge coverage, undercatch bias (Sevruk et al., 2009; Grossi et al., 2017), and oversmoothing of daily spatial variability (Hofstra et al., 2010; Hiebl and Frei, 2018). More recently, ensemble datasets such as E-OBS (Cornes et al., 2018), RhydchprobD (Frei and Isotta, 2019), and FYRE Climate (Devers et al., 2021) have emerged, improving representation of extremes while quantifying uncertainty. But they still fall short in capturing high-elevation precipitation patterns required for mountainous hydrology.

Despite these advances, no existing product simultaneously meets the combined requirements of mountainous hydrology, namely high spatial resolution, long-term coverage, realistic orographic representation, and uncertainty quantification for extreme events. This gap limits our ability to robustly model both seasonal water balances and extreme hydrological events in mountain catchments. This study addresses these shortcomings by introducing a reproducible workflow that combines climatological background fields from the Convection-Permitting Regional Climate Model (CP-RCM) (Caillaud et al., 2021) and conditional geostatistical simulation of daily anomalies to generate ensemble daily precipitation fields. The framework is distributed as a modular open-source code, allowing users to apply it in other regions or update it with new inputs. We ensure reproducibility by delivering ensemble precipitation fields for two years over the Southern Alps, relying solely on openaccess gauge stations. We conduct a multi-perspective evaluation of this product using a diverse set of independent datasets. The novelty of this work does not lie in the individual methods, which are well established, but in their integration into a coherent framework tailored to mountainous regions, the open-source implementation, and the richness of the multi-evaluation. This evaluation encompasses streamflow balances in high-altitude basins, in-situ snow water equivalent sensors, glacier mass balance observations, and daily streamflow time series. The remainder of the paper is structured as follows: Section 2 describes the study domain, the data used for interpolation, and the evaluation datasets. Section 3 presents the interpolation framework and evaluation design. Section 4 reports the evaluation results for hydrological, nivologic, and glaciological applications. Section 5 discusses limitations, perspectives, and reproducibility. Section 6 gives the conclusions.





2 Study domain and hydrometeorological data

2.1 Study domain

The study focuses on the major mountainous regions of France, including the Alps, the Pyrénées, the Massif Central, and the Cévennes. These areas exhibit strong altitudinal gradients (Dura et al., 2024b), which significantly influence precipitation patterns and hydrological processes. The Alps and Pyrénées experience a mix of oceanic and continental influences, with substantial snow accumulation in winter and convective rainfall in summer. The Massif Central and Cévennes are more exposed to Mediterranean influences, leading to intense autumnal precipitation events, particularly in the Cévennes. The observational network used in this study comprises approximately 5,305 rain gauges, from Météo-France and Electricité de France (EDF, the main electricity provider in France), providing daily precipitation from 1982 to 2018. The rain gauge distribution is irregular in space: denser in the Massif Central and the Cévennes, and sparser in the Alps and the Pyrénées. In addition, 14 Cosmic Ray Snow Sensors (in French *Nivomètre à Rayonnement Cosmique*, NRC) (Gottardi, 2009) are distributed in alpine catchments to monitor seasonal SWE, and three glaciers from the GLACIOCLIM observatory network ¹ (namely Saint-Sorlin, Sarennes, Argentière) assess winter accumulation reproduction at high elevations. A subset of 15 catchments, located in the Southern French Alps, where intense convective storms occur primarily during summer and autumn, will be used in hydrological modeling. These catchments are particularly well-suited to assess the ability of precipitation products to reproduce high-intensity events.

2.2 Gridded precipitation products

2.2.1 ERA5-Land

The fifth generation of European ReAnalysis (ERA5-Land, Muñoz-Sabater et al., 2021) is a global reanalysis dataset that simulates atmospheric and surface variables, including precipitation on an hourly basis. It builds upon the atmospheric fields of ERA5 (Hersbach et al., 2020), downscaled to a finer spatial resolution of 9 km. ERA5-Land solely assimilates satellite and radar data and does not include rain gauge measurements. The density and coverage of satellite and radar networks involved in the assimilation, therefore, influence the accuracy of its precipitation estimates (Hassler and Lauer, 2021). Regions such as Central Europe and the United States exhibit higher data quality, compared to more poorly observed areas like tropical oceans.

A key advantage of ERA5-Land is its enhanced spatial resolution, 9 km versus the 31 km resolution of ERA5 or the 80 km of ERA-Interim (Muñoz-Sabater et al., 2021), which contributes to a more accurate representation of precipitation spatial patterns (Gomis-Cebolla et al., 2023).

2.2.2 CERRA-Land

The Copernicus European Regional ReAnalysis Land (CERRA-Land, Ridal et al., 2024) represents the latest regional reanalysis product for Europe, available from 1984 onward at a horizontal resolution of 5.5 km. It employs the HIRLAM ALADIN

¹ https://GLACIOCLIM.osug.fr/





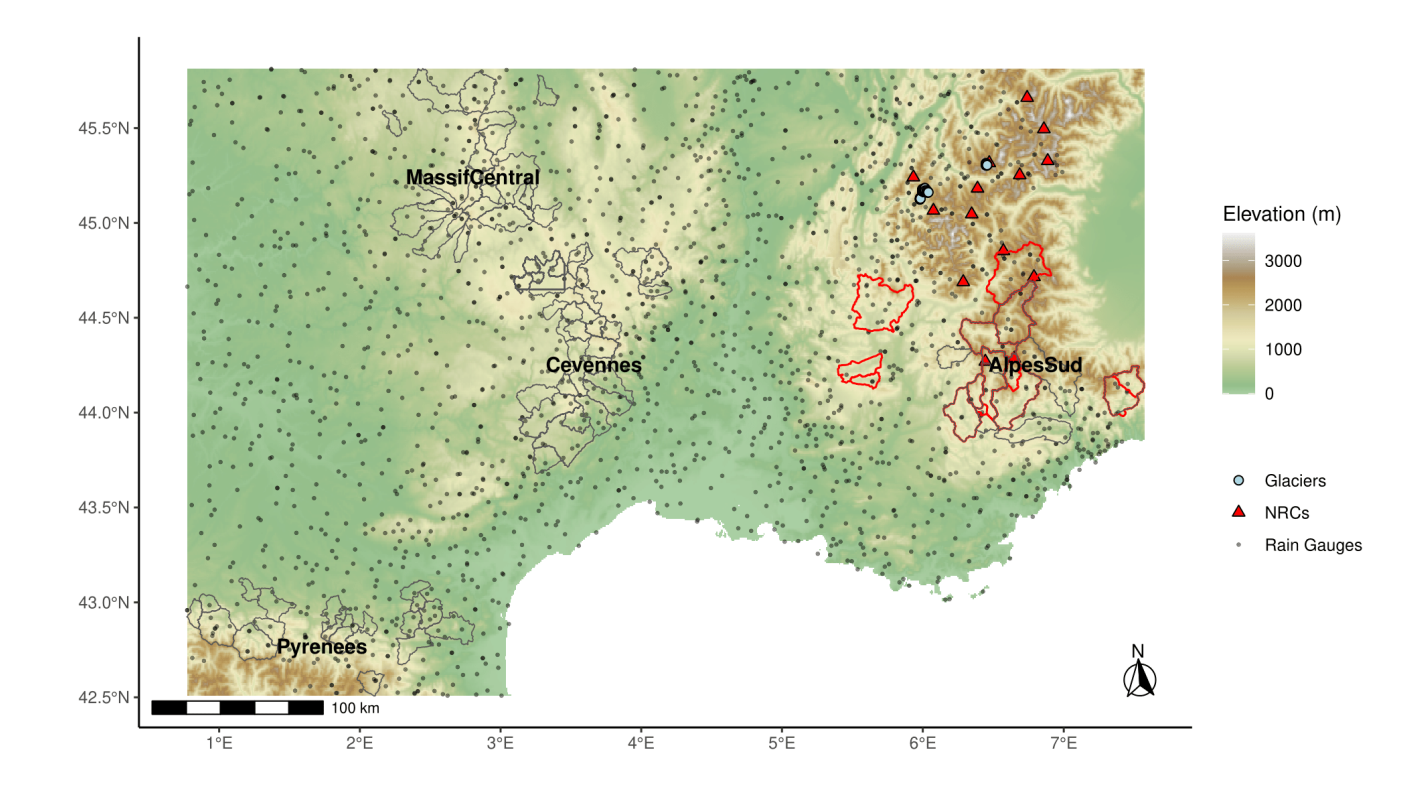


Figure 1. Study domain with elevation (meters). Grey dots indicate rain gauges, light blue dots mark glacier sites, and red triangles show Cosmic Ray Snow Sensors (NRC). Names of major mountain regions and associated catchments are labeled in bold and black, while catchments used for hydrological modeling are highlighted in red. To assess the hydrological mass balance constraints (see sub-section 3.2), 11 (AlpesSud), 46 (Cévennes), 42 (MassifCentral), and 20 (Pyrénées) catchments are colored in grey.

Regional/Mesoscale Operational NWP In Europe (HARMONIE) atmospheric model, driven by ERA5 boundary conditions, and is executed every 3 hours at its native resolution. The MESCAN system (Soci et al., 2016) refines the outputs through optimal interpolation with approximately 8,000 daily rain gauge records. According to Le Moigne (2021), CERRA-Land offers improved representation of snow depth seasonality in the Alps when compared to ERA5-Land.

90 2.2.3 SPAZM

The SPAtialisation en Zones de Montagne (SPAZM) (Gottardi, 2009) is a high-resolution precipitation interpolation tool tailored for mountainous regions. It combines rain gauge measurements with a meteorological background field adjusted





based on topographic features and the prevailing weather type of the day. Using geopotential fields, eight distinct weather patterns are identified (Garavaglia et al., 2010), each associated with a corresponding daily mean precipitation field. Local linear regressions incorporating altitude generate these 1 km spatial resolution fields. For any specific day, the daily observed precipitations are used to derive anomalies, which are interpolated and then applied to the mean precipitation field to obtain the daily precipitation field. Historically, SPAZM integrates data from 2,101 stations operated by EDF (including rain gauges (603) and snow totalizers (216)), Météo-France (555), MeteoSwiss (213), Arpa Piemonte (383), and Instituto Nacional de Méteorologia (131). Although it incorporates fewer stations than COMEPHORE, those used are at higher altitudes. Several hydrological studies (Gottardi, 2009; Ménégoz et al., 2020; Ruelland, 2020) used SPAZM due to its capacity to yield accurate annual precipitation estimates.

subsectionSnow datasets

2.2.4 NRC

The *Nivomètres à Rayonnement Cosmique* (NRCs, Gottardi, 2009) are innovative instruments developed by EDF to monitor SWE using cosmic ray neutron sensing at the daily timescale. These sensors estimate the amount of water stored in the snowpack without the need for snow pits. NRC improves snowpack evolution tracking in the 2,030-2,730 m altitude range for operational hydrological forecasting, especially in the framework of EDF's water resource and hydropower management.

2.2.5 Glacier winter mass balance measurements

Winter Surface Mass Balance (WSMB) data is available for five glaciers, namely Saint-Sorlin, Sarennes, Gebroulaz, Argentière, and Mer de Glace, located throughout the French Alps. These glaciers are part of the GLACIOCLIM observatory (Six and Vincent, 2014). WSMB is measured (in kg×m⁻²) at the end of the snow accumulation season (typically between late April and early May), using snow cores combined with density measurements in both accumulation and ablation zones, with approximately 200 [kg × m⁻²] (200 mm of SWE) uncertainty (Thibert et al., 2008). We exclude the Argentière and Mer de Glace glaciers from the evaluation as the CP-RCM simulations, used in this study, contain artefacts that cause excessive precipitation in the Mont-Blanc area (Monteiro et al., 2022). Measurement points on the three remaining glaciers are located at relatively high elevations, typically between 2,690 and 3,390 m, thus providing valuable information at altitudes not covered by NRCs. For each glacier and accumulation period, we average WSMB measurements because of the small size of the glaciers (≤ 3 km²).

2.3 Hydrological models

120 2.3.1 GR6J

The *Génie Rural à 6 paramètres Journalier* (GR6J, Pushpalatha et al., 2011) is a lumped daily rainfall—runoff model developed in the context of the airGR **R** hydrological modelling package (Coron et al., 2017). It simulates streamflow based on daily precipitation and potential evapotranspiration, using six parameters that control storage, routing, and exchange processes. Its





simplicity and parsimony make it well-suited for large-sample hydrological studies (Tyralis et al., 2023; Devers et al., 2024).

25 GR6J performs well across diverse catchments and climatic conditions (Flores et al., 2021; Kuana et al., 2024; Hrour et al., 2025). We calibrate the model using Kling–Gupta efficiency (Gupta et al., 2009, KGE,) on the daily streamflow.

2.3.2 MORDOR-SD

The MOdèle de RUissellement et de Débit d'ORdre Supérieur – Semi-Distribué (MORDOR-SD) is a semi-distributed conceptual hydrological model, structured by elevation bands, and developed by EDF (Garavaglia et al., 2017) for simulating river discharges at hourly to daily scales. It incorporates snow accumulation and melt, evapotranspiration, soil moisture dynamics, and flow routing. The catchments are discretized based on elevation bands to better simulate snow and rainfall processes. It is particularly suited for mountainous catchments (Evin et al., 2024) and operational use (Paquet, 2004). Calibration uses multi-objective criteria (Garavaglia et al., 2017).

3 Methods

130

135 3.1 Interpolation framework

Interpolating daily precipitation fields over mountainous terrain requires addressing both measurement errors and spatial variability. The proposed methodology involves three main steps:

- (1) correction of gauge undercatch,
- (2) construction of climatological background fields stratified by weather regimes, and
- 140 (3) conditional geostatistical simulation of daily precipitation anomalies.

Figure 2 illustrates the spatial interpolation workflow.

3.1.1 Step 1: Gauge correction

We corrected rain gauge observations for wind-induced undercatch by multiplying all snowfall measurements by 1.6, although undercatch depends on local wind (Sevruk et al., 2009), precipitation intensity (Cauteruccio et al., 2024), gauge type, and also affects rainfall (Pollock et al., 2018). The order of magnitude of 1.6 as a snow correction factor is commonly applied for hydrological and snow applications (e.g. Gottardi, 2009; Jonas and Schirmer, 2022). Daily precipitation at station x_s and day t, denoted $P^{\text{corr}}(x_s, t)$, is corrected for gauge undercatch before interpolation as follows:

$$P^{\text{corr}}(x_s, t) = \alpha_{\text{snow}} \cdot f_{\text{snow}}[T(x_s, t)] \cdot P(x_s, t) + \alpha_{\text{liquid}} \cdot \{1 - f_{\text{snow}}[T(x_s, t)]\} \cdot P(x_s, t)$$

$$\tag{1}$$

where $\alpha_{\rm snow}=1.6$ is the correction factor for solid precipitation and $\alpha_{\rm liquid}=1.0$ for the liquid precipitation. The solid fraction $f_{\rm snow}$ depends on the mean daily temperature $T(x_s,t)$. Appendix A gives more details on the expression of the solid fraction





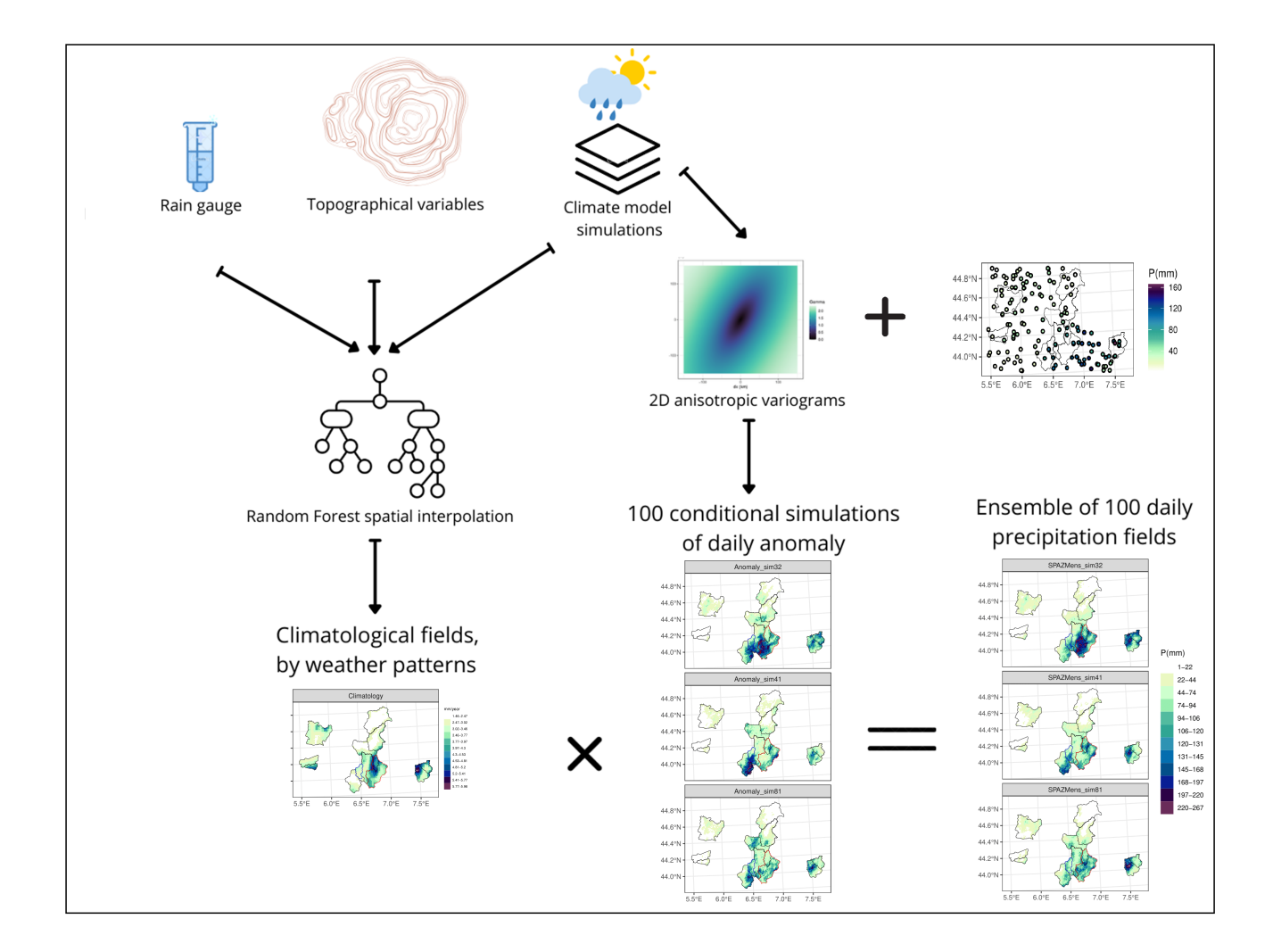


Figure 2. Workflow for generating an ensemble of 100 daily precipitation fields. The process integrates rain gauge undercatch correction, topographical variables, and convection-permitting climate model simulations. These inputs are used in a random forest spatial interpolation to produce climatological fields by weather patterns. Simultaneously, climate model outputs inform 2D daily anisotropic variograms, which are used to generate 100 conditional simulations of daily anomalies. The final ensemble is obtained by multiplying climatological fields with daily anomalies.

given the temperature. Determining appropriate temperature thresholds for rain-snow partitioning remains an active area of research, and the sensitivity to this choice was not evaluated in this study.

3.1.2 Step 2: Climatological construction

155

A key component of the interpolation framework is the use of climatological background fields stratified by class that represent the mean spatial distribution of precipitation and account for orographic effects. These fields are built from CP-RCM simulations





AROME (Caillaud et al., 2021), and refined using long-term rain gauge observations. A machine learning model is used to adjust the model climatology to match observed seasonal totals (Dura et al., 2024a). For each station s and climatological class c (e.g., month, season, or weather regime), the ratio between corrected observations and CP-RCM climatology is $R(x_s,c) = \frac{\overline{P^{\text{corr}}}(x_s,c)}{\overline{M}(x_s,c)}$ where overlines denote climatological averages, and $\overline{M}(x_s,c)$ is the CP-RCM climatology at station x_s . The logratios $\log R(x_s,c)$ are interpolated spatially with a Random Forest regression using the following predictors:

$$\log R(x,c) = f[M(x,c), \log M(x,c), \operatorname{alt}(x), \operatorname{lon}(x), \operatorname{lat}(x), d(x,\mathcal{S})], \tag{2}$$

where alt(x) is the altitude at pixel x, lon(x) is the longitude at pixel x, lon(x) is the latitude at pixel x, lon(x) are buffer distances to the station network \mathcal{S} . We tune the Random Forest algorithm to choose the hyperparameters. Appendix B indicates the hyperparameters tested. We use the ranger (Wright and Ziegler, 2017) package for Random Forest spatial interpolation.

The background field is reconstructed as:

$$B(x,c) = \exp\left[\log R(x,c) + \log M(x,c)\right]. \tag{3}$$

3.1.3 Step 3: Daily anomaly interpolation

Each day t is considered independently. These background fields are then adjusted to match daily rain gauge observations. Anomalies relative to the climatological background are computed as $A(x_s,t) = \frac{P^{\text{corr}}(x_s,t)}{B(x_s,c_t)}$ where c_t is the climatological class of day t. Positive anomalies are transformed into the Gaussian domain through a quantile transformation, which accounts for the skewed nature of precipitation data. Appendix C shows the applied formula for the transformation and back-transformation steps.

The transformed anomalies are modeled as a Gaussian random field as:

$$Z(x,t) = m(x) + \varepsilon(x,t),\tag{4}$$

175

180

165

$$m(x) = \beta_0 + \beta_1 \operatorname{alt}(x) + \beta_2 \operatorname{lon}(x) + \beta_3 \operatorname{lat}(x) + \beta_4 B(x, c_t), \tag{5}$$

where all covariates are standardized. The trend m(x) helps capture large-scale spatial gradients in precipitation while allowing the residual component to model finer-scale variability. Spatial variability of the residuals $\varepsilon(x,t)$ is modeled using a daily anisotropic exponential variogram, estimated from CP-RCM precipitation fields. This allows the interpolation to incorporate directional dependence and reproduce elongated structures typical of convective or orographic precipitation. The exponential variogram is widely adopted in geostatistics (Masson and Frei, 2014; Frei and Isotta, 2019), as it captures the smooth decrease of autocorrelation with distance.

$$\gamma(h) = c_0 + c \left[1 - \exp\left(-\frac{d_{\text{aniso}}(h)}{a} \right) \right],\tag{6}$$





where c_0 denotes the nugget, c the partial sill, a the range parameter, and d_{aniso} the anisotropic distance. Appendix D defines the anisotropic distance. The variogram parameters are optimized by weighted least squares on CP-RCM anomalies, using weights $w(h) = \frac{N_h}{h^2}$, where N_h is the number of pixel pairs separated by distance h..

For each day t, N=100 conditional simulations $\{Z^{(n)}(x,t)\}_{n=1}^N$ are generated with Sequential Gaussian Simulation, conditioned on gauge anomalies, using the *gstat* \mathbf{R} package (Pebesma, 2004). These simulations reproduce both the observed anomaly values and the spatial structure inferred from the variogram and trend, while providing spatial uncertainty. Backtransformation yields N=100 conditional simulations $\{A^{(n)}(x,t)\}_{n=1}^N$ of anomaly fields, and final daily precipitation fields are $\hat{P}^{(n)}(x,t) = A^{(n)}(x,t)B(x,c_t)$. This precipitation product is named *Interpolated Station precipitation for Alpine Regions at Daily resolution* (ISARD).

We use the *raster* \mathbf{Q} (Hijmans, 2025) package to manipulate spatial matrix, *sf* (Pebesma, 2018) and *sp* (Pebesma and Bivand, 2005) \mathbf{Q} packages to deal with spatial point data.

3.2 Evaluation

195

3.2.1 Accumulated precipitation amounts in mountain catchments

To assess the performance of precipitation products in mountainous environments, a two-scale evaluation strategy is applied: one at the catchment scale, utilizing hydrological mass balance constraints, and another at high-altitude point locations using independent snow-related observations.

At the catchment scale, the evaluation is based on the long-term hydrological mass balance. The Turc-Pike models (also known as the Turc or Budyko-type function) (Turc, 1955; Pike, 1964) are widely used to relate runoff (Q) to precipitation (P) and potential evapotranspiration (ETP) via a simple empirical relationship. It expresses the runoff coefficient $\frac{Q}{P}$ as a function of the humidity index $\frac{P}{ETP}$ as follows:

$$\frac{Q}{P} = \left[1 + \left(\frac{P}{ETP}\right)^n\right]^{-\frac{1}{n}}.\tag{7}$$

Q, P, and ETP are in mm.yr $^{-1}$, and n is a shape parameter fitted using least squares, and describing the climate of the catchments. Low n values (≈ 1) are associated with humid climates and energy-limited regimes. High n values (≈ 3) reveal arid or semi-arid regions, where water is limited and potential evapotranspiration exceeds precipitation. For each precipitation product and mountainous region, we compute the deviation of individual catchments from the fitted regional Turc-Pike model, summarized by the sum of squared errors.

210 3.2.2 Accumulated precipitation amounts at high-elevation sites

At high-elevation sites equipped with NRC, seasonal snow accumulation assesses the interannual variability of gridded precipitation products. For each year, we compute the seasonal SWE accumulation as the difference between the maximum and minimum daily SWE values over the winter season (December 1 to February 28). We select the NRC above 2,000 m, where we



215

220

225

230

235



assume negligible melt during winter. Considering the sum of daily SWE variations over a season would relax this assumption, but such comparisons are sensitive to snow redistribution and measurement noise. For each year and precipitation product, the correlation coefficient between accumulated SWE and total precipitation assesses interannual agreement. In the case of the ISARD ensemble, the correlation is computed between the SWE accumulation and the ensemble-mean precipitation. We conduct a similar analysis using winter glacier mass balance data from GLACIOCLIM observatories. Since the measurement dates change each year, precipitation accumulation is computed based on the observed start and end dates of the winter mass balance survey. The correlation between observed glacier winter mass balance and accumulated precipitation provides a complementary evaluation of precipitation products in glacierized environments.

3.2.3 Hydrological modeling of floods

The hydrological models allow the assessment of precipitation intensity and variability at the catchment scale, using measured streamflow as a reference. 15 catchments in the Southern French Alps are selected due to the high occurrence of intense precipitation in summer and autumn. A split-sample approach is applied independently for each catchment and hydrological model. The available simulation period is split into two equal-length sub-periods. For each configuration, the model is calibrated on the first half and evaluated on the second half, then the procedure is reversed. In both cases, one additional year is used as a warm-up period before each calibration or evaluation phase to minimize the influence of initial conditions. We calibrate independently the models for each precipitation forcing. In the case of the 100-member ensemble precipitation forcing, a first calibration is conducted using the ensemble mean precipitation. The resulting parameter set constitutes initial conditions for calibrating each of the 100 individual ensemble members.

Flood events are selected based on the observed discharge time series. We pick an average of three events per year, ensuring a minimum 5-day separation: if multiple events occur within a 5-day window, we retain only the maximum. Additional criteria are applied to ensure the events are rainfall-driven. Specifically, at least one of the two days preceding the flood must exhibit precipitation above the 90th percentile, and the basin-averaged daily air temperature on the flood day must be greater than 0°C.

To evaluate the quality of ensemble streamflow forecasts during flood events, we use the Continuous Ranked Probability Score (CRPS), which measures the distance between a predicted cumulative distribution function (CDF) and an observed scalar value. Let $y_t \in \mathbb{R}$ be the observed streamflow on day t, and $F_t(x)$ the forecasted CDF for that day. The CRPS is defined as:

240
$$CRPS_t = \int_{-\infty}^{+\infty} (F_t(x) - \mathbb{1}_{\{x \ge y_t\}})^2 dx,$$
 (8)

where $\mathbb{1}_{\{x \geq y_t\}}$ is the step function equal to 1 when $x \geq y_t$ and 0 otherwise. We compute CRPS values using the *scoringRules* \mathbf{Q} package (Jordan et al., 2019).

The mean CRPS over the set of flood days in month m, denoted \mathcal{T}_m , is equal to:





$$\overline{\text{CRPS}_m} = \frac{1}{|\mathcal{T}_m|} \sum_{t \in \mathcal{T}_m} \text{CRPS}_t. \tag{9}$$

To compare gridded precipitation products, we compute the Continuous Ranked Probability Skill Score (CRPSS) relative to SPAZM as:

$$CRPSS_m(P \mid SPAZM) = 1 - \frac{\overline{CRPS_m(P)}}{\overline{CRPS_m(SPAZM)}},$$
(10)

where P denotes any gridded precipitation product under evaluation (ERA5-Land, CERRA-Land, ISARD). CRPSS equals 0 indicates similar skill in hydrological modeling of floods to SPAZM. Positive (negative) values indicate improvements (degradation) over SPAZM.

Furthermore, we evaluate how well the model reproduces the distribution of observed streamflows using the Quantile Relative Error (QRE) metric (Evin et al., 2024). This indicator compares the simulated and observed streamflow quantiles and is defined as follows:

$$QRE_p = 1 - \frac{\hat{F}_o^{-1}(p) - \hat{F}_s^{-1}(p)}{\hat{F}_o^{-1}(p)},\tag{11}$$

where $\hat{F}_o^{-1}(p)$ is the empirical distribution of observed streamflows associated with probability p, $\hat{F}_s^{-1}(p)$ is the empirical distribution of simulated streamflows associated with the same probability. QRE below (above) 1 indicates quantile underestimation (overestimation).

4 Results

250

4.1 Accumulated precipitation amounts in mountain catchments

Figure 3 displays the fitted Turc-Pike models, stratified by mountainous regions, for the four precipitation products under consideration. Points located in the red zones correspond to catchments exhibiting non-physical hydrological behavior. Specifically, the annual runoff Q must not exceed the yearly precipitation P, and the difference P - Q (i.e., the water available for evapotranspiration) must not exceed the potential evapotranspiration ETP. For each region and precipitation product, the sum of squared errors (SSE) between individual catchments and the fitted curve can be computed. A lower SSE indicates a better agreement between the precipitation estimates and the expected hydrological behavior of the catchments, assuming that catchments within a given region share similar physical characteristics. The ERA5-Land product underestimates average annual precipitation, resulting in inconsistencies in the hydrological balance. Specifically, the scaled runoff coefficient (Q/P) is too high, and the humidity index (P/ETP) is too low in the Cévennes and Massif Central regions. For instance, the catchment ID 187 situated in the Massif Central is close to 1. In contrast, CERRA-Land shows notable improvements over ERA5-Land, with



280

285

300



point clouds aligning more closely with the Turc-Pike model curves. For example, in the Cévennes, CERRA-Land reduces the sum of squared errors (SSE) from 0.58 to 0.22. SPAZM ranks second among the precipitation products, but its interpolation lacks robustness in the Massif Central, where the SSE reaches 0.16, compared to 0.11 with CERRA-Land. This discrepancy is due to several catchments falling into the red zone, indicating a possible overestimation of annual precipitation. The ISARD product helps reduce the spread of deviations from the Turc-Pike models in all studied regions. In the Pyrénées, ISARD produces more annual precipitation amounts than SPAZM for some high-altitude catchments (ID 118 and 120), reducing SSE from 0.17 to 0.1.

4.2 Accumulated precipitation amounts at high-elevation sites

The Turk-Pike model provides an indirect assessment of the mean precipitation amounts at the catchment scale and over a climatological period, by comparison with long-term means of streamflow measurements and empirical formulations of the evapotranspiration. *In-situ* snow measurements can provide a complementary reference at the point scale and for different years, highlighting interannual variability and systematic biases. Figure 4 displays the reproduction of the inter-annual variability of SWE measurements at (a) NRC and (b) glacier sites.

At NRC sites, the ISARD spread derived from the ensemble often contains the SWE measurements, whereas the other gridded precipitation largely underestimates SWE observations. We find the same ranking of performance as in Fig. 3. ERA5-Land severely underestimates winter precipitation and the inter-annual variability. CERRA-Land shows a notable but insufficient improvement. SPAZM outperforms CERRA-Land only in terms of inter-annual variability, but not in terms of bias. ISARD is the least biased gridded precipitation product, but it overestimates SWE for some NRCs (N1669, N1716). Additionally, it can represent, as does SPAZM, the inter-annual variability of SWE measurements.

Figure 4 (b) provides the same information as Fig. 4 (a) using winter mass balance measured at glaciers as references instead of SWE measurements. The glaciers are slightly at a higher altitude than SWE-measured sites, but the same conclusions remain. ISARD is the most accurate precipitation product, remaining unbiased at Gebroulaz and Saint-Sorlin glaciers, slightly underestimating precipitation at the Sarennes glacier, while effectively capturing the inter-annual variability of the observations.

ISARD is the least biased precipitation product in mountainous regions according to three different data sources: water balance at catchment scale, SWE, and winter mass balance observations. The confidence intervals derived from interpolation uncertainty contain the observations, while not being excessively widespread. We will also evaluate the proposed approach as precipitation input for hydrological modeling to simulate floods.

4.3 Hydrological modeling of floods

4.3.1 Case study

Figure 2 illustrates the spatial interpolation workflow of ISARD for 1996-01-11. The climatological background field is adjusted using 100 conditional simulations of anomaly fields. These anomaly fields show distinct spatial patterns, reflecting interpolation uncertainty, and give precipitation members with associated spatial patterns. The 32nd and 81st members vield



305



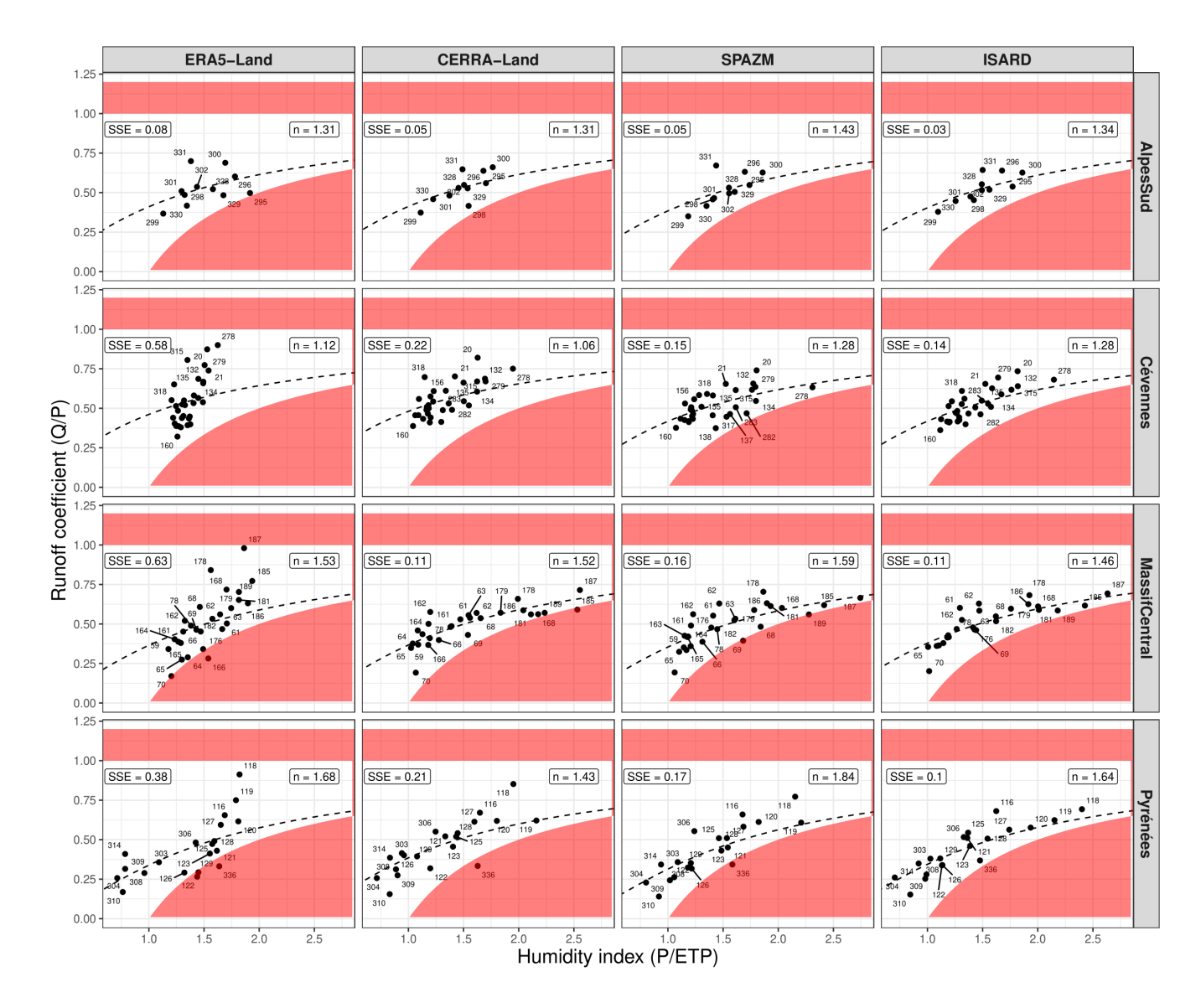


Figure 3. Turc—Pike model results showing the runoff coefficient (y-axis) as a function of the humidity index (x-axis). Black points represent individual catchments. Vertical facets correspond to different regions, and horizontal facets to different gridded precipitation products. Within each facet, the dotted line indicates the fitted Turc—Pike curve, with the fitted parameter n and the sum of squared errors (SSE) reported.

200 mm precipitation cells in the Var at Entrevaux catchment (colored in red), whereas the 41st member exhibits much lower precipitation totals. The members appear less smooth than the deterministic gridded products ERA5-Land, CERRA-Land, and SPAZM, and contain high-intensity cells. The color of the catchments is reflected in the sub-titles of Fig. 6.

Figure 6 illustrates the estimated average precipitation time series for two catchments, along with the associated streamflows derived from hydrological modeling using MORDOR-SD. We focus on the 1991-01-12 flood peak, related to Fig. 5. The





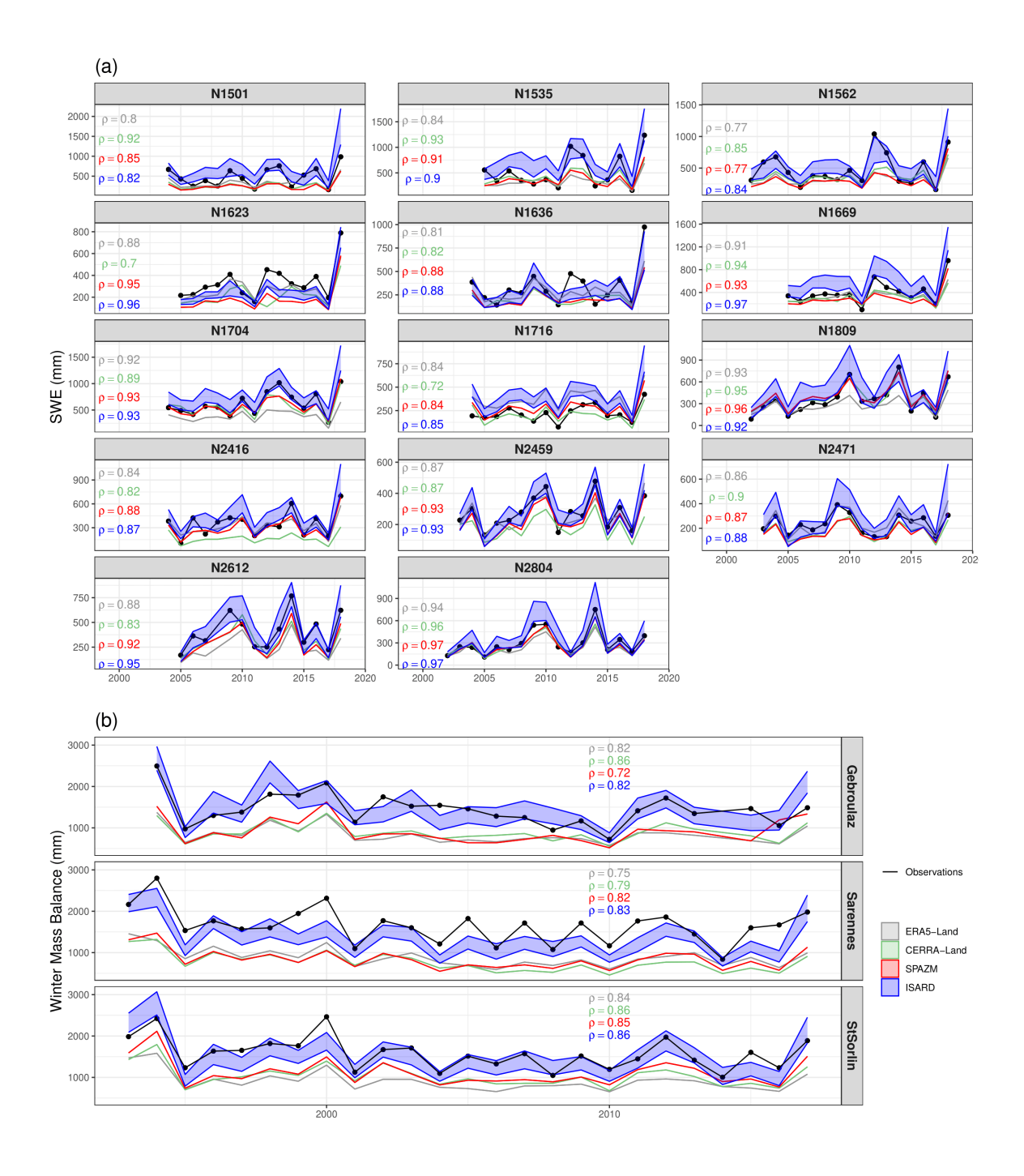
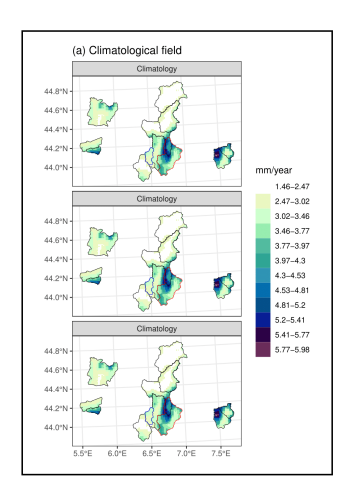
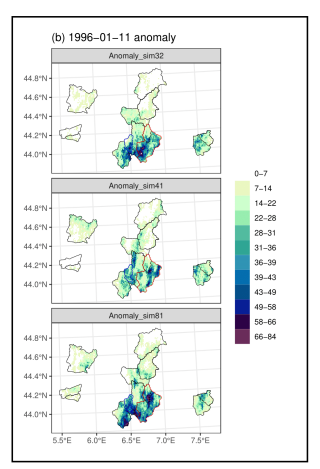


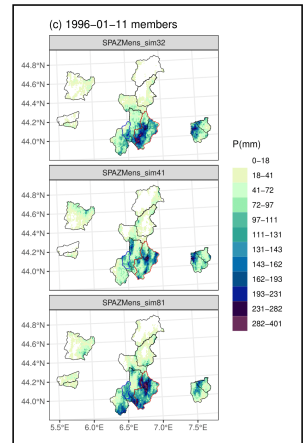
Figure 4. (a) Interannual variability of winter snow water equivalent (SWE) accumulation and accumulated precipitation from 1 December to 28 February, for CERRA-Land, ERA5-Land, SPAZM, and ISARD. Black points denote *in-situ* measurements. (b) Same as (a), but for glacier winter mass balance measurements.











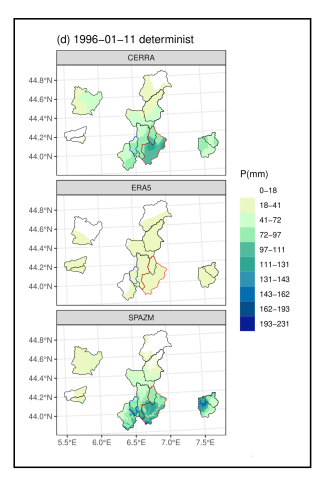


Figure 5. Interpolation workflow illustrated for 11 January 1996. (a) Climatological background field (shown three times for visualization), (b) three randomly selected daily anomaly fields from conditional simulations, and (c) daily precipitation estimates from ERA5-Land, CERRA-Land, SPAZM, and three ensemble members of ISARD corresponding to the simulated anomalies. Catchment outlines are indicated; simulated runoff for the blue and red catchments is presented in Fig. 6.

precipitation uncertainty is significant, even averaged at the catchment scale, and propagates up to hydrological modeling. At the Issole at Mourefrey catchment, the deterministic gridded precipitation products smooth out the spatial variability of the precipitation field, resulting in an underestimation of intense cells, followed by an understimation of the flood peak. On the contrary, ISARD precipitation ranges from 60 to 130 mm. This corresponds to an estimated flood between 25 and 100 m 3 s $^{-1}$, which enables the reproduction of the flood peak, measured at 65 m 3 s $^{-1}$. At the Var at Entrevaux catchment, deterministic products can reproduce the flood peak this time, and some ISARD members show excessive precipitation.

4.3.2 Systematic evaluation

310

315

320

Figure 7 exhaustively evaluates the precipitation products as inputs for hydrological modeling of floods. In Fig. 7 (a), for each catchment, month, and hydrological model, the mean CRPS for floods is computed for both SPAZM and the other precipitation products, with their relative differences shown. Regardless of the catchments, months, and hydrological models considered, SPAZM consistently outperforms ERA5-Land and CERRA-Land in flood modeling. Additionally, the ISARD ensemble outperforms the deterministic SPAZM. We observe substantial improvements in autumn, which is the season most susceptible to flooding due to heavy rainfall. Figure 7 (b) compares the precipitation products in terms of flood distribution. ERA5-Land underestimates the high flood quantiles, across all hydrological models, which is expected and explains the results in Fig. 7 (a). CERRA-Land, in contrast, yields unbiased distribution scores. The poorer CRPS performance relative to SPAZM is therefore not due to a systematic bias in flood quantiles. Despite an improvement in CRPS, ISARD shows similar performance to SPAZM in terms of distribution, with both products being unbiased for large quantiles.





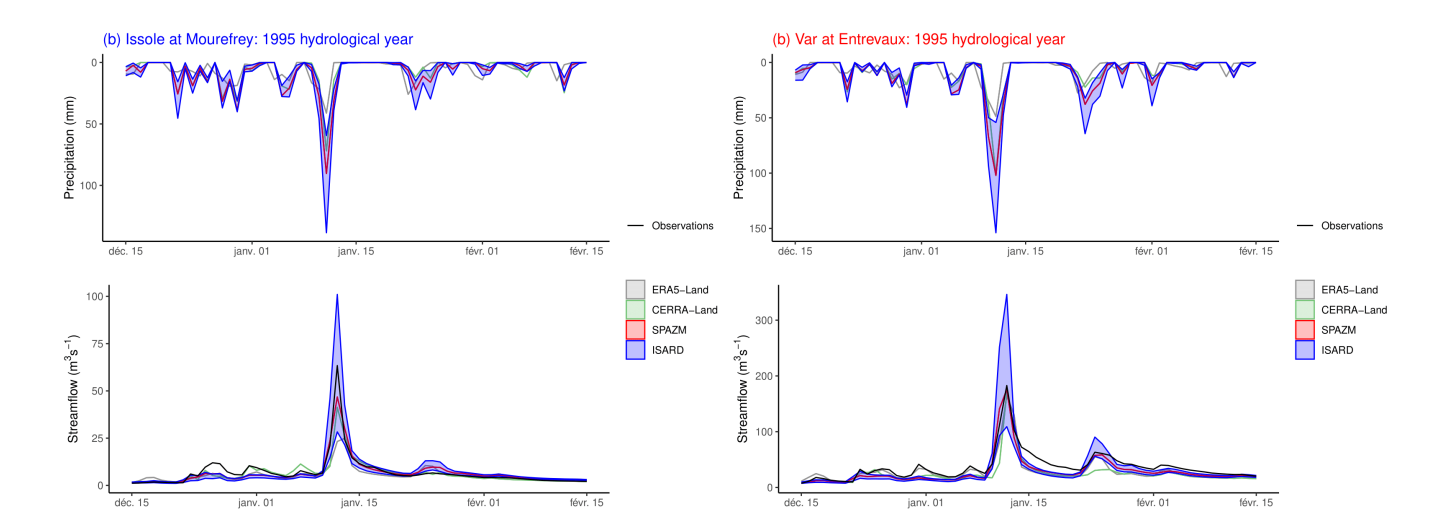


Figure 6. Simulated catchment precipitation and runoff for the 1995 hydrological year (1 September to 31 August), colored by gridded precipitation product, for (a) the Issole at Mourefrey catchment and (b) the Var at Entrevaux catchment. Black curves indicate observed runoff.

5 Discussion

325

5.1 Seasonal accumulation in mountains

The interpolation framework reproduces accumulated precipitation amounts in mountainous regions with good consistency across multiple independent datasets. At the catchment scale, annual precipitation balances well with evapotranspiration and runoff (see Fig. 3). At the point scale, the ensemble reproduces seasonal snow water equivalent (SWE) from nivological reference catchments (NRCs) and winter mass balances of glaciers, providing confidence in the representation of high-elevation precipitation. Despite this overall agreement, some limitations remain:

- **Methodological limitations**: The applied methodology presents two main limitations.
 - Uniform snowfall undercatch correction: To account for the systematic undercatch of snowfall by rain gauges, we applied a uniform correction factor of 1.6 to all snowfall measurements. This choice is consistent with values reported in Alpine studies (Gottardi, 2009; Jonas and Schirmer, 2022), but we emphasize that it represents a coarse approximation. To our knowledge, no operational gridded precipitation product currently includes an explicit undercatch correction. At the seasonal scale, this adjustment largely removes the bias in total snowfall accumulation (see Fig. 4). However, it inevitably compensates both overestimations and underestimations at shorter timescales. In particular, the correction likely misrepresents daily precipitation amounts, since undercatch is not constant but depends on wind speed (Sevruk et al., 2009), precipitation intensity (Cauteruccio et al., 2024), and gauge exposure. Spatial variability is also an issue: in some regions, especially the southernmost NRCs, the correction





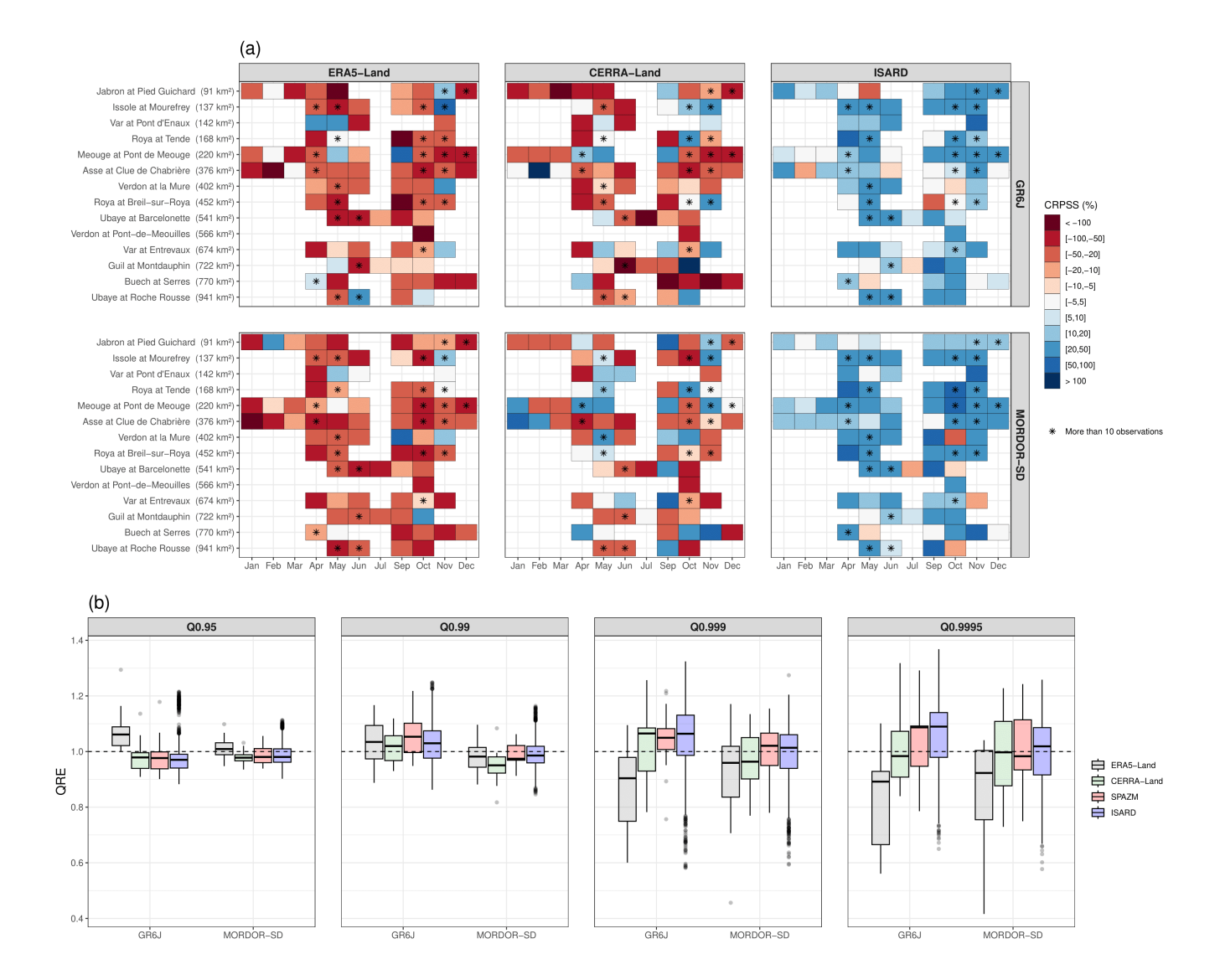


Figure 7. (a) Continuous Ranked Probability Skill Score (CRPSS, % relative to SPAZM) for flood modeling across catchments (y-axis) and months (x-axis), stratified by gridded precipitation products (horizontal facets) and hydrological models (vertical facets). Catchments are ordered by increasing surface area. Box colors correspond to CRPSS values, with red (blue) indicating performance degradation (improvement) relative to SPAZM. Boxes marked with a star indicate more than 10 flood events for the given catchment and month, while empty boxes correspond to fewer than 2 events. (**b)** Distribution of quantile relative errors (y-axis) for the two hydrological models (x-axis), filled by gridded precipitation products and stratified by quantiles (horizontal facets).

appears to produce unrealistically high accumulations. We therefore caution that our corrected dataset should not be interpreted as a physically consistent representation of snowfall at the daily scale. Instead, it should be seen as a first-order seasonal adjustment. Further improvements could rely on more refined transfer functions that explicitly



345

350

355

360



account for wind speed and station metadata (Buisán et al., 2017; Kochendorfer et al., 2020), for example, by exploiting hourly AROME reanalysis winds. The main challenge is the availability and quality of rain gauge metadata, which are often incomplete or subject to change over time.

- Dependence on CP-RCM quality: The reliability of high-altitude precipitation estimates in ungauged regions strongly depends on the capacity of the CP-RCM to reproduce spatial variability in complex mountainous terrain. In particular, the quality of the precipitation–altitude relationship (lapse rates) provided by the CP-RCM is critical. We therefore caution potential users that these lapse rates should always be evaluated before the interpolation step, as illustrated in Dura et al. (2024b). This dependence becomes more pronounced when the rain gauge network is sparse: the sparser the rain gauge network, the more critical the CP-RCM performance becomes.
- Evaluation biases: Some limitations could alter the evaluation of high-altitude precipitation.
 - No-melt assumption: Our evaluation against SWE and glacier mass balances assumes negligible melt during winter. This assumption, historically valid above 2,000 m, is increasingly questionable under present warming. The SWE chronicles of NRC N1669 and N1716 show (not shown here) snow melting in winter, which could explain the supposedly overestimation of ISARD (see Fig. 4). Considering daily SWE variations would relax this assumption, but such comparisons are sensitive to snow redistribution.
 - Scale mismatch: Furthermore, the native resolution of the precipitation ensemble is 1 km, but the resolved resolution is coarser, which is insufficient to explain the spatial variability of snowfall. NRCs are point data, and the Sarennes only covers 0.09 km². This scale mismatch could also explain the differences between precipitation accumulated at the km scale and point SWE measurements, especially in this complex topography area.

5.2 Reproduction of floods using hydrological models

The proposed spatial interpolation framework allows hydrological modeling of floods by providing an ensemble to represent the spatial variability of daily precipitation. The cross-reading of Fig. 5 and Fig. 7 illustrates this point. The ensemble outperforms the best deterministic gridded precipitation products in terms of flood peak representation, but not in long-term runoff frequency distributions. Here are a few points that need to be discussed.

- Model calibration: Hydrological models are recalibrated for each precipitation forcing, which may attenuate differences between the gridded products. We try to mitigate this issue by performing a split-sample evaluation. One possible improvement would be to generate a synthetic reference precipitation field each day, and use it for model calibration. From this field, we could extract several points to act as virtual rain gauges, then apply different spatial interpolation methods to reconstruct the full field. Streamflow simulations could then be performed using the parameters obtained from the full-field calibration, allowing us to assess how interpolation methods affect hydrological performance.
- Hydrological model structure: The models used here are lumped or stratified by elevation bands, which do not fully
 exploit the ensemble's spatial variability. While mean precipitation inputs appear similar across products, spatial patterns

375



380

390

395



differ notably. Fully distributed hydrological models such as MORDOR-TS (Rouhier et al., 2017) would better value the ensemble information and represent the link between spatial rainfall variability and flood response (Bárdossy and Anwar, 2023).

 Evaluation uncertainties: Imperfect hydrological modeling could also contaminate the evaluation of precipitation forcings. Several factors could affect the modeling, such as poor temperature inputs, imperfect evapotranspiration formulation, undercatch of snowfall and rainfall, groundwater exchanges, and hourly hydrological signatures modeled at the daily timescale.

5.3 Scope and reproducibility of the framework

A considerable strength of the framework lies in its reproducibility and applicability across contexts. It requires only rain gauge observations and CP-RCM simulations, making it transferable to regions with varying data availability.

- Station density: We speculate that the interpolation framework is designed for whatever the available rain gauge density, and could also be successful in a low rain gauge density scenario. The construction of the climatological background fields is robust to low station density. The use of Random Forest to interpolate climatological anomalies of rain gauge amounts on CP-RCMs simulations produces unbiased fields even for low rain gauge density, while reproducing the spatial variance of the observations (Dura et al., 2024a). This approach considerably values CP-RCMs simulations, keeping in mind that our ability in precipitation modeling is now outperforming our ability to measure precipitation in mountainous regions (Lundquist et al., 2019). The final step of the interpolation framework, the interpolation of anomalies, is performed through conditional simulations using CP-RCM variograms. As a result, the variogram estimation is not affected by an insufficient rain gauge density, and the interpolation does not produce overly smooth fields (Hofstra et al., 2010). With fewer gauges, the ensemble members diverge more strongly, reflecting actual interpolation uncertainty. In sparser rain gauge networks, generating more members should be considered.
- Flexibility of inputs: While we use CP-RCMs at 2.5 km resolution, the framework might ingest any high-quality RCM depending on the target application scale.
- Extension to other variables: Although developed for daily precipitation, the framework is likely applicable for temperature,
 wind, or radiation. Temperature is less spatially variable and better represented by CP-RCM, while anisotropic variograms support wind interpolation.

Overall, the framework successfully merges point observations and CP-RCM information, providing ensemble precipitation fields that improve hydrological modeling while remaining transparent and reproducible. Its main current limits lie in snowfall undercatch correction, CP-RCM dependence, and evaluation uncertainty, defining clear pathways for future research.





405 6 Conclusion

This study presents a spatial interpolation reproducible workflow applied to daily precipitation in alpine regions. The workflow consists of: (i) correcting rain-gauge measurements for undercatch, (ii) constructing climatological background fields stratified by weather regimes by merging rain gauges with CP-RCM climatologies to account for orographic effects, and (iii) generating conditional simulations of daily anomalies that exploit CP-RCM-derived spatial variability. The approach is benchmarked against widely used products (ERA5-Land, CERRA-Land, and SPAZM, a regression-based interpolator) and evaluated with multiple independent datasets, including catchment-scale water balance, *in-situ* SWE, glacier winter mass balance, and flood hydrological modelling.

Results show that the proposed workflow outperforms existing gridded precipitation products in reproducing seasonal totals in mountainous regions and hydrological modelling of floods. By correcting undercatch and integrating CP-RCM climatology, it provides higher and more realistic precipitation totals at high-elevation sites, while preserving observed interannual variability. The ensemble simulations explicitly represent interpolation uncertainty and capture fine-scale spatial variability, leading to improved flood simulations across all studied catchments and with both hydrological models. Even higher benefits might arise with fully distributed hydrological models.

Overall, these findings highlight the potential of the proposed workflow as a robust approach for precipitation interpolation in regions with complex topography. It is particularly promising in data-scarce areas where high-quality CP-RCM or RCM simulations are available. By providing modular, open-source code and a test case, we ensure the workflow's adaptability to other regions and its extension to diverse climate variables.

Acknowledgements

We are grateful for the AROME simulations provided by Cécile Caillaud and Diego Monteiro.

425 Conflict of interest

The authors declare no conflict of interest.

Code and data availability

AROME is available from the Med CORDEX Portal (https://www.medcordex.eu/search/index.php, last access: 02nd May 2024). The **Q** codes used to perform the analysis are available on the Zenodo repository at https://doi.org/10.5281/zenodo. 17491114 (Dura et al., 2025).





Author contributions

VD conceived the idea, carried out the analysis and wrote the article. GE, DP, and AF participated in the discussion and design of this study and contributed to writing and editing the paper.

Competing interests

435 The authors declare no conflict of interest.

Financial support

This research has been supported by Electricité de France (EDF).





Appendix A: Solid fraction of precipitation

$$f_{snow}[T(x_s,t)] = \begin{cases} 1, & T(x_s,t) < -2^{\circ}C, \\ 0.5 + \frac{T(x_s,t)}{4}, & -2^{\circ}C \le T(x_s,t) \le 2^{\circ}C, , & T(x_s,t) = \frac{T_{min}(x_s,t) + T_{max}(x_s,t)}{2} \\ 0, & T(x_s,t) > 2^{\circ}C. \end{cases}$$
(A1)

440 Appendix B: Random Forest hyperparameters

The Random Forest algorithm hyperparameters are chosen by cross-validation. We perform cross-validation separately for each weather pattern. n_{obs} refers to the number of observations in the training dataset.

- Number of trees $n_{\text{tree}} \in \{50; 100; 500\}$
- Number of co-variables to test to split a leaf $m_{\text{try}} \in \left\{ \frac{n_{obs}}{3}; \frac{n_{obs}}{3}; \frac{n_{obs}}{3} \right\}$
- Number of minimum observations to split a leaf nodesize = 1

Appendix C: Transformation into Gaussian distribution and back-transformation

$$Z_{s,t} = \begin{cases} \Phi^{-1}[u_0 + (1 - u_0)F_{\gamma}(A_{s,t})], & A_{s,t} > 0, \\ \Phi^{-1}[\mathcal{U}(0.01, u_0)], & A_{s,t} = 0, \end{cases}$$
(C1)

where F_{γ} is the Gamma CDF fitted to nonzero values, Φ^{-1} the Gaussian quantile function, u_0 the empirical probability of zero precipitation, and \mathcal{U} is the uniform distribution.

450 Back-transformation yields simulated anomalies

$$A^{(n)}(x,t) = \begin{cases} F_{\gamma}^{-1} \left\{ \frac{\Phi[Z^{(n)}(x,t)] - u_0}{1 - u_0} \right\}, & \Phi[Z^{(n)}(x,t)] > u_0, \\ 0, & \text{otherwise,} \end{cases}$$
 (C2)

Appendix D: Anisotropic distance

The anisotropic distance $d_{\text{aniso}}(h)$ between two locations separated by a lag vector $h = (h_x, h_y)$ is defined as:

$$d_{\text{aniso}}(h) = \sqrt{\left(\frac{h_x \cos \theta + h_y \sin \theta}{a_x}\right)^2 + \left(\frac{-h_x \sin \theta + h_y \cos \theta}{a_y}\right)^2},\tag{D1}$$

with $a_x = a$, $a_y = a/\eta$, η the anisotropy ratio, and θ the anisotropy direction (measured counterclockwise from the x axis).





References

- Berne, A. and Krajewski, W. F.: Radar for hydrology: Unfulfilled promise or unrecognized potential?, Advances in Water Resources, 51, 357–366, https://doi.org/10.1016/j.advwatres.2012.05.005, 2013.
- Buisán, S. T., Earle, M. E., Collado, J. L., Kochendorfer, J., Alastrué, J., Wolff, M., Smith, C. D., and López-Moreno, J. I.: Assessment of snowfall accumulation underestimation by tipping bucket gauges in the Spanish operational network, Atmospheric Measurement Techniques, 10, 1079–1091, https://doi.org/10.5194/amt-10-1079-2017, publisher: Copernicus GmbH, 2017.
 - Bárdossy, A. and Anwar, F.: Why do our rainfall–runoff models keep underestimating the peak flows?, Hydrology and Earth System Sciences, 27, 1987–2000, https://doi.org/10.5194/hess-27-1987-2023, publisher: Copernicus GmbH, 2023.
- Caillaud, C., Somot, S., Alias, A., Bernard-Bouissières, I., Fumière, Q., Laurantin, O., Seity, Y., and Ducrocq, V.: Modelling Mediterranean heavy precipitation events at climate scale: an object-oriented evaluation of the CNRM-AROME convection-permitting regional climate model, Climate Dynamics, 56, 1717–1752, https://doi.org/10.1007/s00382-020-05558-y, 2021.
 - Cauteruccio, A., Chinchella, E., and Lanza, L. G.: The Overall Collection Efficiency of Catching-Type Precipitation Gauges in Windy Conditions, Water Resources Research, 60, e2023WR035 098, https://doi.org/10.1029/2023WR035098, 2024.
- Champeaux, J.-L., Dupuy, P., Laurantin, O., Soulan, I., Tabary, P., and Soubeyroux, J.-M.: Les mesures de précipitations et l'estimation des lames d'eau à Météo-France : état de l'art et perspectives, La Houille Blanche, Numero 5, 28–34, https://doi.org/10.1051/lhb/2009052, 2009.
 - Cornes, R. C., Van Der Schrier, G., Van Den Besselaar, E. J. M., and Jones, P. D.: An Ensemble Version of the E-OBS Temperature and Precipitation Data Sets, Journal of Geophysical Research: Atmospheres, 123, https://doi.org/10.1029/2017JD028200, 2018.
- Coron, L., Thirel, G., Delaigue, O., Perrin, C., and Andréassian, V.: The suite of lumped GR hydrological models in an R package,
 Environmental Modelling & Software, 94, 166–171, https://doi.org/10.1016/j.envsoft.2017.05.002, 2017.
 - Devers, A., Vidal, J.-P., Lauvernet, C., and Vannier, O.: FYRE Climate: a high-resolution reanalysis of daily precipitation and temperature in France from 1871 to 2012, Climate of the Past, 17, 1857–1879, https://doi.org/10.5194/cp-17-1857-2021, 2021.
 - Devers, A., Vidal, J.-P., Lauvernet, C., Vannier, O., and Caillouet, L.: 140-year daily ensemble streamflow reconstructions over 661 catchments in France, Hydrology and Earth System Sciences, 28, 3457–3474, https://doi.org/10.5194/hess-28-3457-2024, 2024.
- Dura, V., Evin, G., Favre, A.-C., and Penot, D.: Spatial Interpolation of Seasonal Precipitations Using Rain Gauge Data and Convection-Permitting Regional Climate Model Simulations in a Complex Topographical Region, International Journal of Climatology, 44, 5745–5760, https://doi.org/10.1002/joc.8662, 2024a.
 - Dura, V., Evin, G., Favre, A.-C., and Penot, D.: Spatial variability in the seasonal precipitation lapse rates in complex topographical regions application in France, Hydrology and Earth System Sciences, 28, 2579–2601, https://doi.org/10.5194/hess-28-2579-2024, 2024b.
- 485 Dura, V., Evin, G., Favre, A.-C., and Penot, D.: ISARD code and input data, Zenodo, https://doi.org/10.5281/zenodo.17491114, 2025.
- Evin, G., Le Lay, M., Fouchier, C., Penot, D., Colleoni, F., Mas, A., Garambois, P.-A., and Laurantin, O.: Evaluation of hydrological models on small mountainous catchments: impact of the meteorological forcings, Hydrology and Earth System Sciences, 28, 261–281, https://doi.org/10.5194/hess-28-261-2024, publisher: Copernicus GmbH, 2024.
- Fantini, A., Raffaele, F., Torma, C., Bacer, S., Coppola, E., Giorgi, F., Ahrens, B., Dubois, C., Sanchez, E., and Verdecchia, M.: Assessment of multiple daily precipitation statistics in ERA-Interim driven Med-CORDEX and EURO-CORDEX experiments against high resolution observations, Climate Dynamics, 51, 877–900, https://doi.org/10.1007/s00382-016-3453-4, 2018.



505



- Faure, D., Delrieu, G., and Gaussiat, N.: Impact of the Altitudinal Gradients of Precipitation on the Radar QPE Bias in the French Alps, Atmosphere, 10, 306, https://doi.org/10.3390/atmos10060306, 2019.
- Flores, N., Rodríguez, R., Yépez, S., Osores, V., Rau, P., Rivera, D., and Balocchi, F.: Comparison of Three Daily Rainfall-Runoff
 Hydrological Models Using Four Evapotranspiration Models in Four Small Forested Watersheds with Different Land Cover in SouthCentral Chile, Water, 13, 3191, https://doi.org/10.3390/w13223191, number: 22 Publisher: Multidisciplinary Digital Publishing Institute,
 2021.
 - Frei and Isotta: Ensemble Spatial Precipitation Analysis From Rain Gauge Data: Methodology and Application in the European Alps, JGR Atmospheres, https://doi.org/10.1029/2018JD030004, place: Suisse Zurich, 2019.
- Garavaglia, F., Gailhard, J., Paquet, E., Lang, M., Garçon, R., and Bernardara, P.: Introducing a rainfall compound distribution model based on weather patterns sub-sampling, Hydrology and Earth System Sciences, 14, 951–964, https://doi.org/10.5194/hess-14-951-2010, publisher: Copernicus GmbH, 2010.
 - Garavaglia, F., Le Lay, M., Gottardi, F., Garçon, R., Gailhard, J., Paquet, E., and Mathevet, T.: Impact of model structure on flow simulation and hydrological realism: from a lumped to a semi-distributed approach, Hydrology and Earth System Sciences, 21, 3937–3952, https://doi.org/10.5194/hess-21-3937-2017, publisher: Copernicus GmbH, 2017.
 - Gomis-Cebolla, J., Rattayova, V., Salazar-Galán, S., and Francés, F.: Evaluation of ERA5 and ERA5-Land reanalysis precipitation datasets over Spain (1951–2020), Atmospheric Research, 284, 106 606, https://doi.org/10.1016/j.atmosres.2023.106606, 2023.
 - Gottardi, F.: Estimation statistique et réanalyse des précipitations en montagne. Utilisation d'ébauches par types de temps et assimilation de données d'enneigement. Application aux grands massifs montagneux français, phdthesis, Institut National Polytechnique de Grenoble INPG, https://tel.archives-ouvertes.fr/tel-00419170, 2009.
 - Grossi, G., Lendvai, A., Peretti, G., and Ranzi, R.: Snow Precipitation Measured by Gauges: Systematic Error Estimation and Data Series Correction in the Central Italian Alps, Water, 9, 461, https://doi.org/10.3390/w9070461, number: 7 Publisher: Multidisciplinary Digital Publishing Institute, 2017.
- Gugerli, R., Gabella, M., Huss, M., and Salzmann, N.: Can Weather Radars Be Used to Estimate Snow Accumulation on Alpine Glaciers? An

 Evaluation Based on Glaciological Surveys, Journal of Hydrometeorology, https://doi.org/10.1175/JHM-D-20-0112.1, section: Journal of Hydrometeorology, 2020.
 - Gupta, H. V., Kling, H., Yilmaz, K. K., and Martinez, G. F.: Decomposition of the mean squared error and NSE performance criteria: Implications for improving hydrological modelling, Journal of hydrology, 377, 80–91, 2009.
- Hassler, B. and Lauer, A.: Comparison of Reanalysis and Observational Precipitation Datasets Including ERA5 and WFDE5, Atmosphere, 12, 1462, https://doi.org/10.3390/atmos12111462, number: 11 Publisher: Multidisciplinary Digital Publishing Institute, 2021.
 - Hersbach, H., Bell, B., Berrisford, P., Hirahara, S., Horányi, A., Muñoz-Sabater, J., Nicolas, J., Peubey, C., Radu, R., Schepers, D., Simmons, A., Soci, C., Abdalla, S., Abellan, X., Balsamo, G., Bechtold, P., Biavati, G., Bidlot, J., Bonavita, M., De Chiara, G., Dahlgren, P., Dee, D., Diamantakis, M., Dragani, R., Flemming, J., Forbes, R., Fuentes, M., Geer, A., Haimberger, L., Healy, S., Hogan, R. J., Hólm, E., Janisková, M., Keeley, S., Laloyaux, P., Lopez, P., Lupu, C., Radnoti, G., de Rosnay, P., Rozum, I., Vamborg, F.,
- Villaume, S., and Thépaut, J.-N.: The ERA5 global reanalysis, Quarterly Journal of the Royal Meteorological Society, 146, 1999–2049, https://doi.org/10.1002/qj.3803, 2020.
 - Hiebl, J. and Frei, C.: Daily precipitation grids for Austria since 1961—development and evaluation of a spatial dataset for hydroclimatic monitoring and modelling, Theoretical and Applied Climatology, 132, 327–345, https://doi.org/10.1007/s00704-017-2093-x, 2018.
 - Hijmans, R. J.: raster: Geographic Data Analysis and Modeling, https://rspatial.org/raster, r package version 3.6-32, 2025.



540

545



- Hofstra, N., New, M., and McSweeney, C.: The influence of interpolation and station network density on the distributions and trends of climate variables in gridded daily data, Climate Dynamics, 35, 841–858, https://doi.org/10.1007/s00382-009-0698-1, 2010.
 - Hrour, Y., Thomas, Z., Rousseau-Gueutin, P., Ait-Brahim, Y., and Fovet, O.: Enhancing hydrological modeling with bias-corrected satellite weather data in data-scarce catchments: a comparative analysis of SWAT and GR4J models, Frontiers in Water, 7, https://doi.org/10.3389/frwa.2025.1582589, publisher: Frontiers, 2025.
- Jiang, Y., Yang, K., Qi, Y., Zhou, X., He, J., Lu, H., Li, X., Chen, Y., Li, X., Zhou, B., Mamtimin, A., Shao, C., Ma, X., Tian, J., and Zhou, J.: TPHiPr: a long-term (1979–2020) high-accuracy precipitation dataset (1/30°, daily) for the Third Pole region based on high-resolution atmospheric modeling and dense observations, Earth System Science Data, 15, 621–638, https://doi.org/10.5194/essd-15-621-2023, 2023.
 - Jonas, T. and Schirmer, M.: Enhance existing Swiss precipitation products with particular regards to snowfall, Final report, Federal Office of Meteorology and Climatology (MeteoSwiss) and Swiss Federal Institute for Forest, Snow and Landscape Research (WSL), project completed under GCOS–CH and GAW–CH support, 2022.
 - Jordan, A., Krüger, F., and Lerch, S.: Evaluating Probabilistic Forecasts with scoringRules, Journal of Statistical Software, 90, 1–37, https://doi.org/10.18637/jss.v090.i12, 2019.
 - Kochendorfer, J., Earle, M. E., Hodyss, D., Reverdin, A., Roulet, Y.-A., Nitu, R., Rasmussen, R., Landolt, S., Buisán, S., and Laine, T.: Undercatch Adjustments for Tipping-Bucket Gauge Measurements of Solid Precipitation, Journal of Hydrometeorology, https://doi.org/10.1175/JHM-D-19-0256.1, section: Journal of Hydrometeorology, 2020.
 - Kuana, L. A., Almeida, A. S., Mercuri, E. G. F., and Noe, S. M.: Regionalization of GR4J model parameters for river flow prediction in Paraná, Brazil, Hydrology and Earth System Sciences, 28, 3367–3390, https://doi.org/10.5194/hess-28-3367-2024, publisher: Copernicus GmbH, 2024.
 - Le Moigne, P.: Documentation of the CERRA-Land system, Tech. rep., Météo-France, 2021.
- Lundquist, J., Abel, M. R., Gutmann, E., and Kapnick, S.: Our Skill in Modeling Mountain Rain and Snow is Bypassing the Skill of Our Observational Networks, Bulletin of the American Meteorological Society, https://doi.org/10.1175/BAMS-D-19-0001.1, 2019.
 - Masson, D. and Frei, C.: Spatial analysis of precipitation in a high-mountain region: exploring methods with multi-scale topographic predictors and circulation types, Hydrology and Earth System Sciences, 18, 4543–4563, https://doi.org/10.5194/hess-18-4543-2014, 2014.
 - Monteiro, D., Caillaud, C., Samacoïts, R., Lafaysse, M., and Morin, S.: Potential and limitations of convection-permitting CNRM-AROME climate modelling in the French Alps, International Journal of Climatology, 42, 7162–7185, https://doi.org/10.1002/joc.7637, 2022.
 - Muñoz-Sabater, J., Dutra, E., Agustí-Panareda, A., Albergel, C., Arduini, G., Balsamo, G., Boussetta, S., Choulga, M., Harrigan, S., Hersbach, H., Martens, B., Miralles, D. G., Piles, M., Rodríguez-Fernández, N. J., Zsoter, E., Buontempo, C., and Thépaut, J.-N.: ERA5-Land: a state-of-the-art global reanalysis dataset for land applications, Earth System Science Data, 13, 4349–4383, https://doi.org/10.5194/essd-13-4349-2021, 2021.
- Ménégoz, M., Valla, E., Jourdain, N. C., Blanchet, J., Beaumet, J., Wilhelm, B., Gallée, H., Fettweis, X., Morin, S., and Anquetin, S.: Contrasting seasonal changes in total and intense precipitation in the European Alps from 1903 to 2010, Hydrology and Earth System Sciences, 24, 5355–5377, https://doi.org/10.5194/hess-24-5355-2020, publisher: Copernicus GmbH, 2020.
 - Paquet, E.: Evolution du modèle hydrologique MORDOR : modélisation du stock nival à différentes altitudes, La Houille Blanche, pp. 75–82, https://doi.org/10.1051/lhb:200402008, number: 2 Publisher: EDP Sciences, 2004.
- Pebesma, E.: Simple Features for R: Standardized Support for Spatial Vector Data, The R Journal, 10, 439–446, https://doi.org/10.32614/RJ-2018-009, 2018.





- Pebesma, E. J.: Multivariable geostatistics in S: the gstat package, Computers & Geosciences, 30, 683–691, https://doi.org/10.1016/j.cageo.2004.03.012, 2004.
- Pebesma, E. J. and Bivand, R.: Classes and methods for spatial data in R, R News, 5, 9-13, https://CRAN.R-project.org/doc/Rnews/, 2005.
- Pike, J. G.: The estimation of annual run-off from meteorological data in a tropical climate, Journal of Hydrology, 2, 116–123, https://doi.org/10.1016/0022-1694(64)90022-8, 1964.
 - Pollock, M. D., O'Donnell, G., Quinn, P., Dutton, M., Black, A., Wilkinson, M. E., Colli, M., Stagnaro, M., Lanza, L. G., Lewis, E., Kilsby, C. G., and O'Connell, P. E.: Quantifying and Mitigating Wind-Induced Undercatch in Rainfall Measurements, Water Resources Research, 54, 3863–3875, https://doi.org/10.1029/2017WR022421, 2018.
- Pushpalatha, R., Perrin, C., Le Moine, N., Mathevet, T., and Andréassian, V.: A downward structural sensitivity analysis of hydrological models to improve low-flow simulation, Journal of Hydrology, 411, 66–76, https://doi.org/10.1016/j.jhydrol.2011.09.034, 2011.
 - Quéno, L., Vionnet, V., Dombrowski-Etchevers, I., Lafaysse, M., Dumont, M., and Karbou, F.: Snowpack modelling in the Pyrenees driven by kilometric-resolution meteorological forecasts, The Cryosphere, 10, 1571–1589, https://doi.org/10.5194/tc-10-1571-2016, publisher: Copernicus GmbH, 2016.
- Ridal, M., Bazile, E., Le Moigne, P., Randriamampianina, R., Schimanke, S., Andrae, U., Berggren, L., Brousseau, P., Dahlgren, P., Edvinsson, L., El-Said, A., Glinton, M., Hagelin, S., Hopsch, S., Isaksson, L., Medeiros, P., Olsson, E., Unden, P., and Wang, Z. Q.: CERRA, the Copernicus European Regional Reanalysis system, Quarterly Journal of the Royal Meteorological Society, 150, 3385–3411, https://doi.org/10.1002/qj.4764, _eprint: https://rmets.onlinelibrary.wiley.com/doi/pdf/10.1002/qj.4764, 2024.
- Rouhier, L., Le Lay, M., Garavaglia, F., Le Moine, N., Hendrickx, F., Monteil, C., and Ribstein, P.: Impact of mesoscale spatial variability of climatic inputs and parameters on the hydrological response, Journal of Hydrology, 553, 13–25, https://doi.org/10.1016/j.jhydrol.2017.07.037, 2017.
 - Ruelland, D.: Should altitudinal gradients of temperature and precipitation inputs be inferred from key parameters in snow-hydrological models?, Hydrology and Earth System Sciences, 24, 2609–2632, https://doi.org/10.5194/hess-24-2609-2020, 2020.
 - Sevruk, B., Ondrás, M., and Chvíla, B.: The WMO precipitation measurement intercomparisons, Atmospheric Research, 92, 376–380, https://doi.org/10.1016/j.atmosres.2009.01.016, 2009.
 - Sideris, I. V., Gabella, M., Erdin, R., and Germann, U.: Real-time radar-rain-gauge merging using spatio-temporal co-kriging with external drift in the alpine terrain of Switzerland, Quarterly Journal of the Royal Meteorological Society, 140, 1097–1111, https://doi.org/10.1002/qj.2188, 2014.
- Six, D. and Vincent, C.: Sensitivity of mass balance and equilibrium-line altitude to climate change in the French Alps, Journal of Glaciology, 60, 867–878, https://doi.org/10.3189/2014JoG14J014, 2014.
 - Soci, C., Bazile, E., Besson, F., and Landelius, T.: High-resolution precipitation re-analysis system for climatological purposes, Tellus A: Dynamic Meteorology and Oceanography, 68, 29 879, https://doi.org/10.3402/tellusa.v68.29879, 2016.
 - Thibert, E., Blanc, R., Vincent, C., and Eckert, N.: Glaciological and volumetric mass-balance measurements: error analysis over 51 years for Glacier de Sarennes, French Alps, Journal of Glaciology, 54, 522–532, https://doi.org/10.3189/002214308785837093, 2008.
- Turc, L.: Le bilan d'eau des sols : relations entre les précipitations, l'évaporation et l'écoulement, https://www.persee.fr/doc/jhydr_0000-0001_1955_act_3_1_3278, publisher: Persée Portail des revues scientifiques en SHS, 1955.
 - Tyralis, H., Papacharalampous, G., and Khatami, S.: Expectile-based hydrological modelling for uncertainty estimation: Life after mean, Journal of Hydrology, 617, 128 986, https://doi.org/10.1016/j.jhydrol.2022.128986, 2023.





- Vidal, J.-P., Martin, E., Franchistéguy, L., Baillon, M., and Soubeyroux, J.-M.: A 50-year high-resolution atmospheric reanalysis over France with the Safran system, International Journal of Climatology, 30, P. 1627, https://doi.org/10.1002/joc.2003, 2010.
 - Vionnet, V., Six, D., Auger, L., Dumont, M., Lafaysse, M., Quéno, L., Réveillet, M., Dombrowski-Etchevers, I., Thibert, E., and Vincent, C.: Sub-kilometer Precipitation Datasets for Snowpack and Glacier Modeling in Alpine Terrain, Frontiers in Earth Science, 7, https://doi.org/10.3389/feart.2019.00182, publisher: Frontiers, 2019.
- Wright, M. N. and Ziegler, A.: ranger: A Fast Implementation of Random Forests for High Dimensional Data in C++ and R, Journal of Statistical Software, 77, 1–17, https://doi.org/10.18637/jss.v077.i01, 2017.